17

Rapid Nanoparticle Characterization

Rajasekhar Anumolu[1] and Leonard F. Pease III[1,2,3]
[1]*Department of Chemical Engineering, University of Utah, Salt Lake City, UT*
[2]*Department of Internal Medicine, Division of Gastroenterology, Hepatology, and Nutrition, University of Utah, Salt Lake City, UT*
[3]*Department of Pharmaceutics and Pharmaceutical Chemistry, University of Utah, Salt Lake City, UT*
USA

1. Introduction

Nanoparticles are the focus of intense scientific and engineering attention, due to their unique properties and wide array of potential biomedical, optical, and electronic applications. Their unique properties bridge those of bulk materials and atomic or molecular structures. Whereas bulk materials display constant physical properties regardless of size, nanomaterial properties may be size-dependent, such as quantum confinement in semiconductor particles, surface plasmon resonance in many metal particles and superparamagnetism in magnetic materials. However, design, synthesis, and fabrication of nanoparticles for specific applications or fundamental inquiry remains immature without accurate and well resolved characterization of nanoparticle size and structure. To date, nanoparticles may be characterized using a variety of traditional techniques including electron microscopy (EM), atomic force microscopy (AFM), dynamic and static light scattering (DLS and SLS), x-ray photoelectron spectroscopy (XPS), powder X-ray diffraction (XRD), Fourier transform infrared spectroscopy (FTIR), size exclusion chromatography (SEC), asymmetric flow field flow fractionation (AFFFF), X-ray crystallography, small angle neutron scattering (SANS), matrix-assisted laser desorption/ionization time-of-flight mass spectrometry (MALDI-TOF), ultraviolet-visible spectroscopy, dual polarization interferometry, and nuclear magnetic resonance (NMR) [Attri & Minton, 2005; Bondos, 2006; Casper & Clug, 1962; Chang et al., 1992; Colter & Ellem, 1961; Dai et al., 2008; Kim et al., 2010; Knapman et al., 2010; Pease et al., 2009; Russel et al., 1989; Shoemaker et al., 2010; Siuzdak et al., 1996; Swann et al., 2004; Umbach et al., 1998; Wang, 2005]. However, techniques such as electron microscopy and X-ray crystallography are expensive, time consuming, and require extensive computational resources. Other techniques such as SANS also suffer from limited availability [Kuzmanovic et al., 2008]. Despite the wide array of available techniques, there remains a need for rapid, label free, and statistically powerful characterization techniques to resolve dynamic multimodal distributions within approximately an hour or less.

Electrospray differential mobility analysis (ES-DMA) is a rapid technique (analysis time scales on the order of 1-100 min) with sub-nanometer resolution. ES-DMA can detect

particles from 0.7 nm – 700 nm [Hollertz et al., 2011; Tsai et al., 2008]. At its smallest, ES-DMA has sub-angstrom resolution on the molecular diameter. ES-DMA can be used to determine the concentration of nanoparticles and also deposit the nanoparticles for additional characterization. ES-DMA is particularly attractive because it operates at atmospheric pressure and requires neither fluorescent tagging nor calibration curves. It separates particles based on their charge-to-size ratio, similar to mass spectrometry or capillary electrophoresis but without the expensive equipment such as turbo pumps [Pease et al., 2008]. While ES-DMA does not possess the atomic scale resolution of X-ray crystallography, EM, or SANS, its simplicity gives it decided advantages in speed, cost, and statistical significance [Pease et al., 2011]. The "coarse-grain" structures it resolves provide significant information regarding the structure of several biological particles such as assembling viruses, virus-like particles, and vaccines for biomedical applications and the structure of nanoparticle clusters and aggregates [Cole et al., 2009; Hogan et al., 2006; Lute et al., 2008; Thomas et al., 2004; Wick et al., 2005].

Here we review this label-free, quantitative, and rapid technique that provides full multimodal size distributions with sub-nanometer resolution. We first describe the operation and physics underlying this instrument. We then describe exemplary applications of this instrument to nanoparticle characterization. We finally conclude by comparing ES-DMA to several of the techniques listed above and provide an outlook for future growth of the technique.

1.1 ES-DMA – operation and physics

In ES-DMA, also referred to as a scanning mobility particle sizing (SMPS) or gas-phase electrophoretic mobility molecular analysis (GEMMA) [Bacher et al., 2001; Saucy et al., 2004], a particle suspension is first conveyed into the gas phase (Figure 1 shows ES-DMA system components). This is achieved by electrospray ionization, which produces a narrow distribution of droplets, typically 150-400 nm in initial diameter.

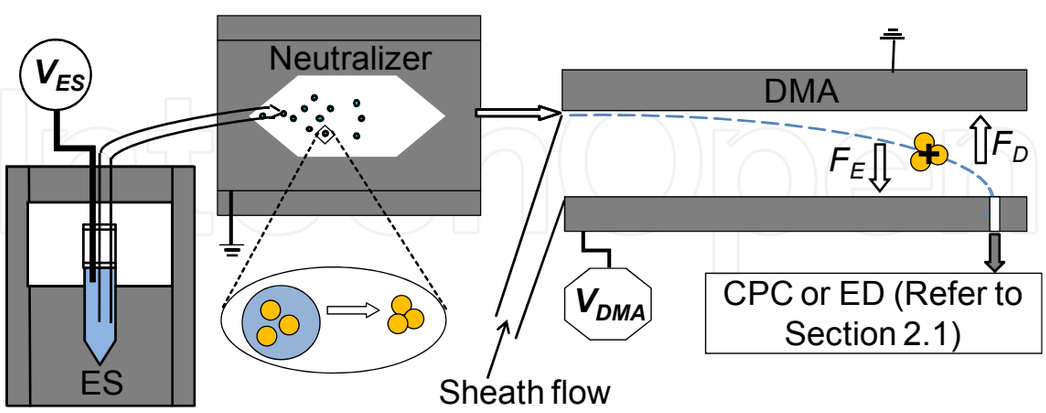

Fig. 1. Schematic of ES-DMA nanoparticle characterization system. ES-DMA produces either a size distribution using an ultrafine condensation particle counter (CPC) or deposits nanoparticles using an electrostatic deposition (ED) chamber as discussed in Section 2.1. Here, F_E is the electrostatic force and F_D is the radial component of drag force acting on the nanoparticle system.

The electrospray system uses pressure (3-5 psig) to drive flow through a 25-40 micron inner diameter capillary. At the capillary tip, a Taylor cone forms due to an applied electric field (1-3.7 kV across ~0.3 cm). Droplets emitted from the cone encapsulate one or multiple discrete nanoparticles (e.g. DNA coated gold nanoparticles or recombinant polymer strands) and are entrained in a mixed stream of air (1.0 L/min) and carbon dioxide (0.2 L/min) at atmospheric pressure. The droplets quickly evaporate leaving a dry nanoparticle. For example, Figure 1 shows three gold nanoparticles forming into a trimeric cluster. As these drying particles pass through a neutralizing chamber, collisions with charged ions reduce the charge on the nanoparticle received in the electrospray to a modified Boltzmann distribution [Kaddis et al., 2007; Loo et al., 2005; Wiedensohler, 1988]. Consequently, the positively charged particles analyzed in the DMA carry predominantly a single net positive charge. Within the annular DMA analysis chamber, a potentiated (≤-10 kV) center electrode attracts charged particles dragged towards the exit of the DMA by a carrier gas (nitrogen). The electrical force acting on the particles carrying n_e electron charges of magnitude e (=1.602 x 10^{-19} C) through an electric field, E_s, is given by $F_E = n_e e E_s$. The mobility of the particle, Z_p, is then defined as the ratio of the particle's velocity v to the force giving rise to that velocity [Anumolu et al., 2011; Knutson & Whitby, 1975]. This force gives rise to a resulting radial drag force acting on the particle, $F_D = 3\pi\mu_g v d_p / C_c$, where d_p is the spherically equivalent particle mobility diameter and μ_g is the gas viscosity. This form of Stokes' Law corrects for moderate to high Knudsen number flow using the Cunningham slip correction factor, C_c, because many particle sizes are equal to or less than the mean free path of air, λ (=66 nm) [Radar, 1990]. This correction factor is given by $C_c = 1 + Kn\ [a + \beta \exp(-\gamma/Kn)]$, where $Kn = 2\lambda/d_p$, $a = 1.257$, $\beta = 0.40$, and $\gamma = 1.110$ [Allen & Raabe, 1985; Radar, 1990]. When the particles are not spherical, several authors show that the drag force in the free molecular regime (where Kn>1) depends on the projected area [Epstein, 1924; Hollertz et al., 2011; Pease et al., 2011]. Particles quickly reach their terminal velocity in a small fraction of the particle's DMA residence time allowing us to equate the radial component of the two forces to obtain the particle's electrical mobility as

$$Z_p = \frac{n_e e C_c}{3\pi\mu_g d_p}. \tag{1}$$

The instrument also has a unique mobility, which holds for any laminar velocity profile, given by [Knutson & Whitby, 1975],

$$Z_p^* = \frac{(q_a - q_s)/2 + q_{sh}}{2\pi V L} \ln\frac{r_2}{r_1}, \tag{2}$$

where, V is the average voltage on the center electrode, q_{sh} is the sheath flow, q_s is the sampling or monodispersed flow out of the DMA, q_a is the aerosol flow out of the ES into the DMA, L is the length between polydisperse aerosol inlet and exit slit (4.987 cm), r_1 is the inner radius of annular space of the DMA (0.937 cm), and r_2 is the outer radius of annular space of the DMA (1.905 cm). Here the values of L, r_1, and r_2 represent the dimensions of nano-DMA. When the particle and instrument mobilities are equal, the particle passes through a collection slit at the distal end of the center electrode to be counted or further

analyzed. Combining particle and instrument mobilities determines the mobility diameter of the particle to be

$$\frac{d_p}{C_c} = \frac{2n_e eVL}{3\mu_g q_{sh} \ln\left(\frac{r_2}{r_1}\right)}. \tag{3}$$

Here C_c is grouped with the diameter d_p, because C_c is diameter dependent. Stepping through a series of voltages (or sizes) while counting with a condensation particle counter (CPC), yields a complete multimodal distribution. The continuous and high throughput (millions of particles per run) design of the instrument ensures statistical significance of both mean and tails of ES-DMA size distributions. The distributions are also highly repeatable with a standard deviation on the number-average diameter of only ± 0.1 nm for nominally 10 nm gold nanoparticles [Pease et al., 2007].

By collecting data for several seconds and averaging over time the mean or number–average diameter may be calculated with $d_{ave} = \sum_i N_i d_i / \sum_i N_i$, where N_i is the number of particles counted by the CPC of size d_i [Fissan et al., 1983]. Because we apply a negative bias to ions within the DMA, only particles that acquire a positive charge are detected. A modified expression for the Boltzmann distribution [Weidensohler, 1988] is used to correct for this effect, transforming the distribution of positively charged particles into the complete distribution of all particles regardless of charge. The fraction of singly and doubly charged particles was determined by Weidensohler,

$$f(j) = 10^{\sum_{l=0}^{5} a_l^j [\log(d_p / d_o)]^l}, \tag{4}$$

where d_p represents the mobility diameter of the particle, d_o = 1 nm, j is the number of charges on a particle, and a_o^1 through a_5^1 are -2.3484, 0.6044, 0.4800, 0.0013, -0.1553, and 0.0320, while a_o^2 through a_5^2 are -44.4756, 79.3772, -62.8900, 26.4492, -5.7480, and 0.5049, respectively, based on the probability of charging provided by Fuchs [Fuchs, 1963]. To remove the influence of doubly counted particles from the size distribution, the charge corrected count is multiplied by the overlap factor, f_{no}, which becomes unity for d_p < 5 nm and $10.94/d_p - 29.94/d_p^2$ for d_p > 5 nm as described by Pease, et al. [Pease et al., 2010a].

Alternatively, monodispersed nanoparticles or nanoparticle clusters from the DMA (or polydispersed nanoparticles bypassing the DMA) may be directed into an electrostatic deposition (ED) chamber. Within the chamber an electrode beneath a collecting substrate exerts an electrostatic field (≤-10 kV over ~2.5 cm) to attract entering particles. Electrostatic deposition is particularly effective at assembling nanoparticles onto the substrates, in contrast to impaction, because nanoparticle electrical mobilities are high (Eq. 1) and their inertia is relatively low (i.e., the Stokes number of nanoparticles remains much less than unity) such that they follow gas streamlines in the absence of an external field [Hinds, 1999]. Several factors affect the collection efficiency with smaller particles, higher particle charging, higher applied voltage, and lower gas flow rates increasing deposition. Figure 2 shows that smaller nanoparticles indeed have higher deposition

efficiency (~100% when d < 30 nm) [Dixkens & Fissan, 1999]. The electrode features also affect the deposition profiles. For example, smaller electrodes lead to more focused deposition.

Fabrication of nanoparticle-based devices requires addressing nanoparticles to specific locations, which may be accomplished using electrostatic forces. For instance, several authors have demonstrated that charged nanoparticles may be directed to specific substrate locations by tuning electric fields near surfaces using charge patterning [Barry et al., 2003a, 2003b; Fissan et al., 2003; Jacobs et al., 2002; Krinke et al., 2002, 2003]. Similarly, Tsai, et al., used planar p-n junction patterned substrates to generate an array of tunable electric fields [Park & Phaneuf, 2003; Tsai et al., 2005]. Several other substrates are used for electrostatic deposition such as TEM grids (~3 mm in diameter) with thin holey carbon films [Anumolu et al., 2011], silicon wafers, and glass substrates pretreated in KOH and UVO-cleaner [Kang et al., 2011, 2012]. The optimum deposition time onto holey carbon TEM grids requires the product of the aerosol number density and time to exceed 3000 particle·hr/cm^3, while ~100 particle·hr/cm^3 is optimal to prepare glass rounds for precision optical measurements. Pease, et al., used freshly cleaved mica surfaces for deposition of carbon nanotubes for AFM observation [Pease et al., 2009b]. More recently, Saffari, et al., deposited particles into live DU145 prostate cancer cells in culture stored in Petri dishes [Hedieh et al., 2012].

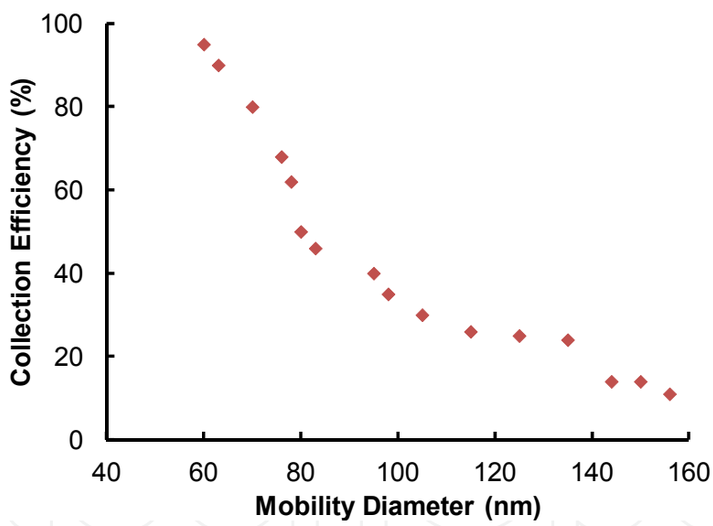

Fig. 2. Nanoparticle collection efficiency via ED at 1 L/min of inlet flow and 10 kV [Adapted from Dixkens & Fissan, 1999].

1.1.1 Predicting molecular size and structure

Bacher, et al., correlated empirically the mobility diameter (d_p in nm) of a variety of large biomolecules including proteins, antibodies, and viral proteins with their molecular weight, M_w (in kDa), assuming proteins to be globular spheres of constant density. Their composite empirical expression, $M_w = -22.033 + 9.830d_P - 1.247d_P^2 + 0.228\, d_P^3$ (which when inverted for d_P becomes $d_P = 1.832M_W^{0.3256} \approx (6M_w/\pi\rho)^{1/3}$ [Pease et al., 2001], where ρ is the density of protein), predicted individual protein and protein aggregates sizes [Bacher et

al., 2001]. Pease, et al., demonstrated how to convert the projected areas, A_i, of DNA coated gold particles into d_p, accounting for Brownian motion in the DMA [Pease et al., 2007] with

$$d_p = \left(\frac{\pi^{1/2}}{6} \sum_{i=1}^{3} A_i^{-1/2} \right)^{-1} . \tag{5}$$

This equation may be applied to a wide variety of biomolecules using coordinates from the protein databank to obtain the projected areas. For example, Pease, et al., used protein databank coordinates to predict the ES-DMA measured size of IgG antibodies and insulin oligomers within 1 nm [Pease et al., 2008, 2010c]. Additionally, this formula may be used to characterize the icosahedral structure of viruses by converting the ES-DMA measured size into the edge-to-edge lengths of regular icosahedra [Pease et al., 2011]. The equation also accommodates more challenging geometries such as nanorods, clusters composed of heterogeneously sized nanospheres, and clusters composed of both nanospheres and nanorods [Pease et al., 2010a, 2010b]. Pease further extended this formulation to determine the selectivity of specific cluster compositions (dimers, trimers, etc.), as will be discussed subsequently [Pease, 2011a].

2. Materials characterized by ES-DMA

A wide variety of materials have been characterized by ES-DMA including gold nanoparticles, nanotubes (e.g. single wall carbon nanotubes), nanorods (e.g. gold nanorods), bionanoparticles (polymers, proteins, viruses, etc.), functionalized nanoparticles (e.g. with DNA), quantum dots, aggregated and conjugated nanoparticles, etc. Here we review the contributions of ES-DMA to the characterization of these materials.

2.1 Gold and metallic nanoparticles

Gold nanoparticles remain among the most extensively analyzed materials by ES-DMA because they are very stable, inert and (by many definitions) biocompatible. Figure 3 shows the size distribution of nominally 15 nm gold nanoparticles and the TEM image of size-separated gold nanoparticles using ES-DMA. The National Institute of Standards and Technology (NIST) and the Nanotechnology Characterization Lab (NCL) issued a Joint Assay Protocol, "PCC-10: Analysis of Gold Nanoparticles by Electrospray Differential Mobility Analysis (ES-DMA)," which details a protocol for size analysis of liquid borne gold nanoparticles via ES-DMA [Pease et al., 2010d]. The use of ES-DMA to measure the size distribution of colloidal nanoparticles was first demonstrated well over a decade ago [Juan & Fernandez de la Mora, 1996]. Since then gold and silver nanoparticles have been analyzed using ES-DMA [Elzey & Grassian, 2010; Lenggoro et al., 2002, 2007] by comparing with colloids of known sizes, such as polystyrene particles. However, polystyrene particles are not monodispersed. In 2007, NIST issued 10 nm, 30 nm, and 60 nm gold nanoparticles as official NIST reference materials, which are very monodispersed and can replace polystyrene particles for DMA calibration. Various techniques including DLS, EM, and SAXS were used to characterize these gold nanoparticles, and the diameter of gold nanoparticles measured by each of the different techniques was in reasonable agreement

with ES-DMA (see Section 3). These reference materials were issued at the behest of the National Cancer Institute (NCI) to evaluate and qualify the methodology and instrument performance related to the physical characterization of nanoparticle systems.

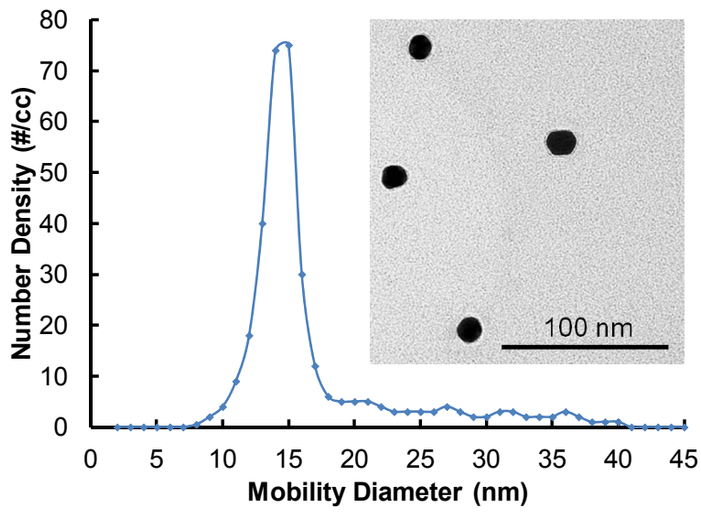

Fig. 3. ES-DMA size distribution and the TEM image (inset) following electrostatic deposition of gold nanoparticles nominally 15 nm in diameter. Number density is the number of particles per cubic centimeter of gas flow through the CPC at a rate of 1.5 L/min.

2.2 Nanotubes and nanorods

Characterization of non-spherical particles is of immense interest, as the shape of a particle along with its size greatly influences particle properties (optical, mechanical, etc.). Though several techniques are available to quantify the length distributions of nanorods and nanotubes, ES-DMA remains competitive (see Section 3 for a detailed comparison). Several authors have reported the characterization of rod- or tube-like particles, such as, gold nanorods and multi-walled carbon nanotubes [Baron et al., 1994; Chen et al., 1993; Deye et al., 1999; Kim & Zachariah, 2005, 2006, 2007a; Moisala et al., 2005; Song et al., 2005]. Song, et al., used a shape factor analysis to convert the average mobility diameter into the average length of gold nanorods. Kim, et al., used Dahneke's theory to convert ES-DMA mobility size distributions into length distributions [Kim et al., 2007b]. Their adaptation includes the orientation of the nanowire as a key factor. Below 70 nm Brownian motion randomizes the orientation of the particles, whereas longer particles align with the electric field in DMA. Pease, et al., used ES-DMA to characterize rapidly the length distribution of single-walled carbon nanotubes from liquid suspensions [Pease et al., 2009b]. Their model, also based on Dahneke's theory, converts the mobility diameter distribution to a length distribution but also accounts for thin salt layers present on the nanotubes that form during electrospray. They found d_{nt}, the diameter of an individual nanotube, and d_s, the diameter of a spherical salt particle, to be key parameters in their model. Figure 4 shows the conversion of mobility size into length distribution based on nanotube diameter and salt layer thickness. Figure 4 also suggests that neglecting to correct for the salt layer overestimates the nanotube length by 42 nm to 56 nm, whereas a small increase in d_{nt} (from 1.4 nm to 2 nm) for a 20 nm

mobility diameter results in a decrease in carbon nanotube length of 71 nm [Pease et al., 2009b].

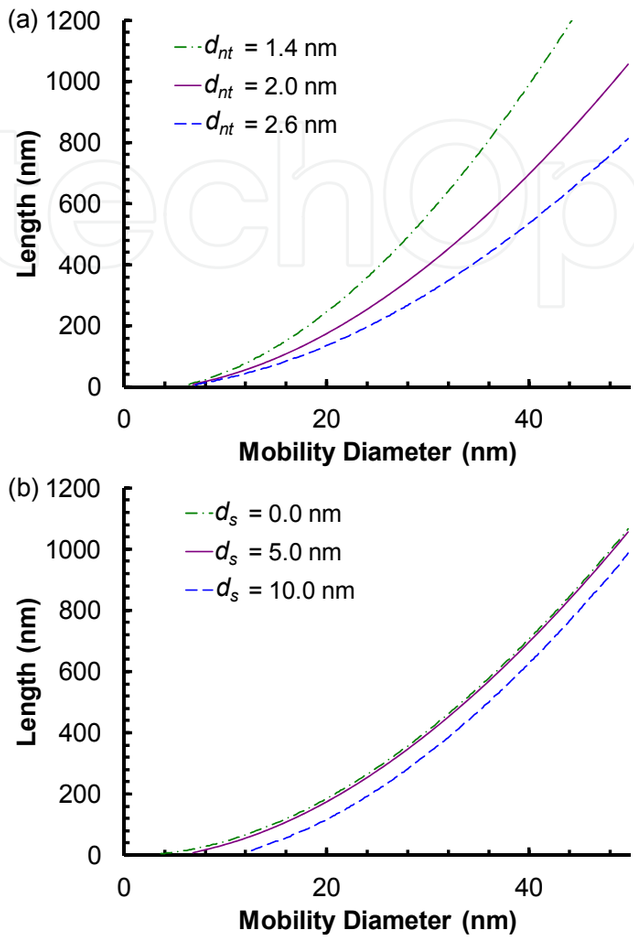

Fig. 4. Length of carbon nanotubes versus mobility diameter as a function of nanotube diameter, d_{nt}, and salt particle size, d_s, for (a) d_{nt} values of 1.4 nm (dash dot), 2.0 nm (solid), and 2.6 nm (long dash) with d_s = 5.0 nm; (b) for d_s = 0.0 nm (dash dot), 5.0 nm (solid), and 10.0 nm (long dash) with d_{nt} = 2.0 nm. Reprinted with permission from [Pease et al., 2009b]. Copyright (2009) Wiley-Interscience.

2.3 Bionanoparticles

Biological systems are of immense interest and ES-DMA is perfectly suited to analyze their soft components. Several biological particles such as viruses, proteins, and protein polymers have soft structures for which ES-DMA is sufficiently gentle to preserve their structure.

2.3.1 Viral nanoparticles

Despite the importance of viral structure, very few methods quantify or validate it. ES-DMA has been demonstrated to be gentle for both enveloped viruses and protein complexes [Wick et al., 2005]. For instance, Wick, et al., used ES-DMA to measure the enveloped alpha virus

to be 70 nm ± 3 nm in good agreement with that reported in the structural databases of viruses (~70 nm), indicating electrospray and neutralizer to be sufficiently gentle to preserve the lipid envelop despite shear forces present in the Taylor cone at exit of the electrospray capillary. Furthermore, Hogan, et al., and Thomas, et al., have shown that icosahedral viruses remain infectious following electrospray [Hogan et al., 2006; Thomas et al., 2004].

Pease, et al., demonstrated that the ES-DMA technique can be used to quantify the dimensions of icosahedral viruses [Pease et al., 2011]. A recent review highlights the use of ES-DMA to analyze virus particles [Pease, 2012]. Previous ES-DMA studies of viruses report only the mobility diameter, neglecting the inherent geometry of the virus [Bacher et al., 2001; Hogan et al., 2006; Lute et al., 2008; Thomas et al., 2004]. This left the connection between mobility and actual dimensions of the virus unclear and poorly defined. Pease, et al., converted the mobility diameter, d_p, into the icosahedral geometry expected of *Tectiviridae* viruses using the projected area formulation introduced previously [Pease et al., 2010a]. Figure 5 shows the three orthogonal projections for icosahedra and also gives the corresponding projected areas, where a represents the length of an edge between neighboring vertices.

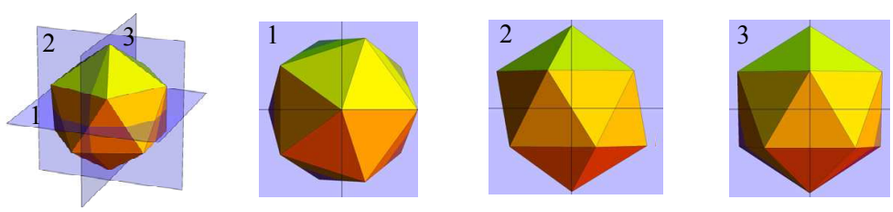

Fig. 5. Three orthogonal projections and projected areas for an icosahedron. Here, $A_1 = 5a^2/(2(5-\sqrt{5}))^{1/2}$, $A_2 = (2+\sqrt{5})a^2/2$, $A_3 = a^2((25+11\sqrt{5})/10)^{1/2}$. Reprinted with permission from [Pease et al., 2011]. Copyright (2011) American Chemical Society.

Figure 6 shows serial ES-DMA size distributions of a PR772 virus sample tracking the temporal disintegration of the capsid. The primary capsid peak in the size distribution was identified at 61.4 nm, allowing determination of the symmetry and the number of major capsid proteins per capsid. Capsomers and capsomer assemblies were identified by estimating their mobility diameter via Eq. 5 using coordinates from the protein data bank [Pease et al., 2010a]. Figure 6 also provides insight into the mechanism of degradation. Initial degradation products take the form of mostly individual capsomers though some larger assemblies (peak at 18.6 nm) are observed. Continued loss of smaller pieces leaves partially degraded capsids (peak at 51.6 nm). The small but nonzero number density between 20 and 40 nm suggests a continuum of degradation products. However, only after many weeks do the individual capsomers begin to breakdown as seen by the appearance of peaks <7 nm at t = 20 weeks.

2.3.2 Polymeric nanoparticles

Nanoparticles hold potential for a variety of biomedical applications including targeted gene and drug delivery. However, most nanoparticles with refined size (*i.e.*, where the ratio of standard deviation in the diameter to the mean diameter, also called coefficient of variation, is <0.15) are metallic with potential *in vivo* toxicity issues (e.g. quantum dots,

silver particles, *etc.*) [Elzey & Grassian, 2010; Pease, 2011a]. Anumolu, et al., fabricated nanoparticles using ES-DMA from recombinant silk elastin-like protein polymers (SELPs) by encapsulating multiple polymer strands in evaporating electrospray droplets. SELPs were selected because they showed promise in clinical trials for localized gene delivery (i.e. by direct injection into tumor containing tissue) [Gustafson & Ghandehari, 2010].

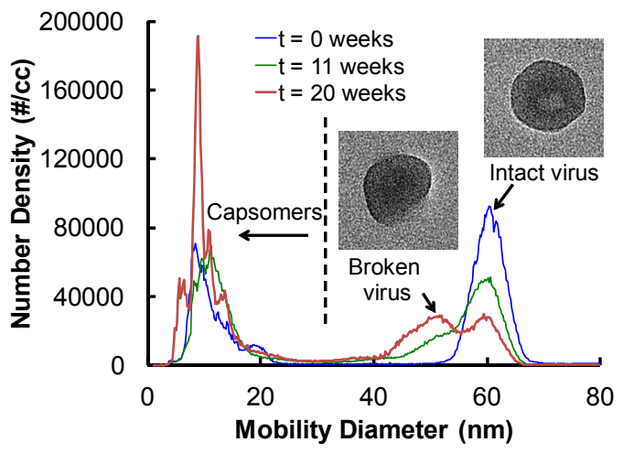

Fig. 6. Serial ES-DMA size distributions of a single PR772 sample showing the disintegration of the capsid (61.4 nm) at t = 0 weeks (short dash), 11 weeks (solid), and 20 weeks (long dash) after storage at room temperature. The number density was corrected with a modified Boltzmann distribution [Wiedensohler, 1988] to reconstruct the full size distribution. Insets are TEM images of representative capsids electrostatically collected at (a) 61.4 nm and (b) 50.0 nm without fixing or stain. Reprinted with permission from (Pease et al., 2011). Copyright (2011) American Chemical Society.

A key feature of their work is the use of the DMA to purify the particles. Figure 7a shows that prior to separation in the DMA, the particles are heterogeneous in size, but after separation the distributions narrow dramatically. Indeed, Figure 7b shows two histograms of SELP particles nominally 24.0 nm and 36.0 nm in diameter, each assembled from nearly 200 nanoparticle TEM images. Statistical compilation shows the standard deviation on the diameter of these purified particles to be 1.2 nm and 1.4 nm for the two sizes, respectively, leading to coefficients of variation of <5% [Anumolu et al., 2011]. This manufacturing precision meets or exceeds that of metallic nanoparticles and rivals that of biologically assembled particles such as viruses [Cole et al., 2009; Lute et al., 2008; Pease, 2011a; Pease et al., 2007]. These results provide the first compelling evidence that ES-DMA can both *generate* and *purify* polymeric nanoparticles with high dimensional uniformity without the addition of hazardous solvents.

These highly uniform nanoparticles may be developed into carriers of therapeutic agents [Anumolu et al., 2011]. Simply including the therapeutic agent in the polymer solution to be electrosprayed, leads to incorporation within the nanoparticle. For example, SELP-815K was mixed with plasmid DNA and fluorescein isothiocyanate (FITC). In both cases new peaks arise 7-8 nm from the primary peak and the distribution of all particles is wider, confirming incorporation of these model agents of gene and drug delivery.

Combining precise control over nanoparticle size with precise control over polymer structure enabled by recombinant techniques presents a unique opportunity to precisely tune the payload and rate of release of the therapeutic agents as well as their biological fate.

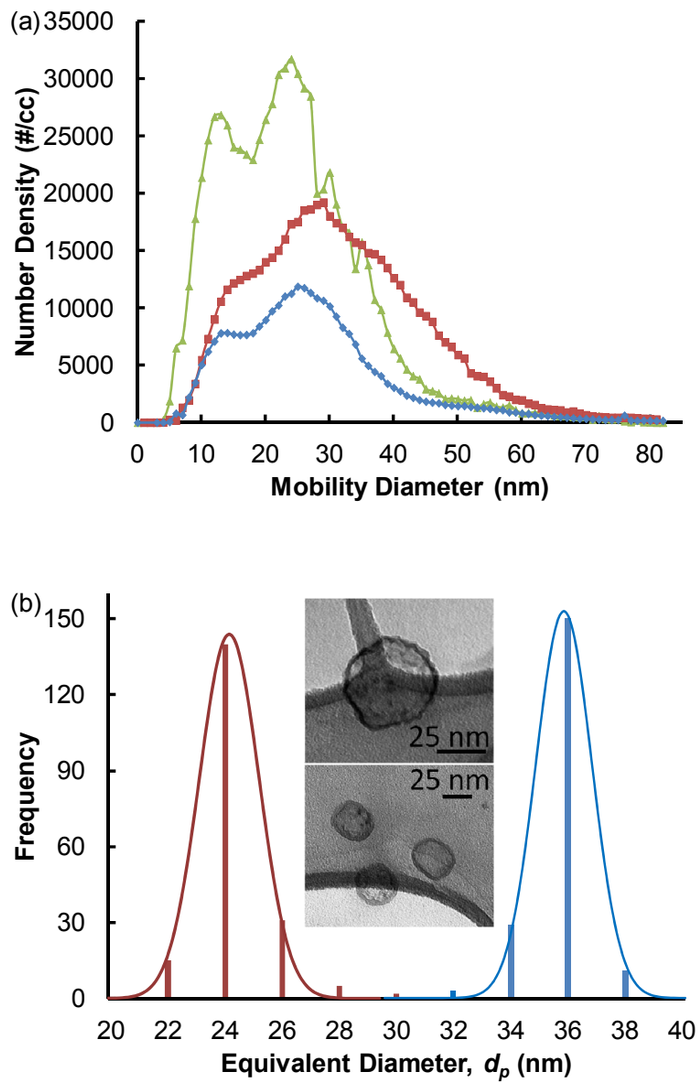

Fig. 7. (a) Size distributions of nanoparticles fabricated from polymers SELP-815K (▲), SELP-415K (■), and SELP-47K (♦) at a polymer weight fractions and buffer concentrations of 0.00133 and 2 mM, respectively. The designation 815K indicates that the strands are assembled from multiple consecutive repeats of 8 silk units, 15 elastin units, and one lysine modified elastin. (b) Histograms representing the diameter of SELP-815K nanoparticles as determined from TEM following electrostatic deposition of nominally 24.0 nm and 36.0 nm. The mean and standard deviation of the size distribution of these particles are 24.2 ± 1.2 nm and 35.8 ± 1.4 nm, respectively. The insets show micrographs of SELP-415K nanoparticles electrostatically collected on TEM grids. Reprinted with permission from [Anumolu et al., 2011]. Copyright (2011) American Chemical Society.

2.4 Surface-functionalized nanoparticles

Determining the surface density of ligands attached to nanoparticle surfaces is a challenging problem in nanoscience and nanotechnology and a major barrier to commercial development. Pease, et al., used ES-DMA to determine the surface density of thiol terminated single-stranded DNA (ssDNA) tethered to 20 nm gold nanoparticles. Comparing the diameter of coated and bare particles (Figure 8a) shows that ES-DMA measured sizes are sensitive to *both* hard and soft components of complex nanoparticles. Pease, et al., investigated the dependence of the coating thickness on the number of deoxythymine (dT) nucleotides or bases, N_b, within a ssDNA strand. The dependence of the coating thickness on N_b is related to the spatial configuration of the bases within the strand in the dry state. If the strands pack together tightly in a brush structure, similar to alkanethiol self-assembled monolayers, the coating thickness should scale linearly on the length of the ssDNA backbone [Tsai et al., 2008]. However, if packing allows for sufficient space between the strands, the bases may adopt a random coil configuration to maximize entropy (appropriate for dried strands) such that the coating thickness is proportional to the linear end-to-end distance to the ½ power. Other exponents are available for hydrated or collapsed configurations due to interactions with solvent, if present. Figure 8b shows that the data follow square root curve fits, indicating that the strands adopt a random coil configuration on the nanoparticle surface [Adamuți-Trache et al., 1996; Netz & Andelman, 2003; Russel et al., 1989]. Knowing the configuration of the strands enables estimation of the surface density because the drag force experienced by the coated particle in the DMA depends on the diameter of the particle, the projected area of the coiled strands, and the number of those strands on the surface. The "lumpy sphere" model combines these variables by approximating each strand as a hemispherical cap, enabling direct determination of the surface density [Mansfield, 2007]. The reported densities are in reasonably agreement with those for "brushes" prepared under similar conditions [Demers et al., 2000; Liao & Roberts, 2006; Petrovykh et al., 2006; Xu & Craig, 2007]. Tsai, et al., used a similar strategy to determine the size, thermal stability, and surface density of alkanethiol self-assembled monolayers (SAMs) on gold nanoparticles. They measured the coating thickness and binding energy of SAMs with excellent precision [Tsai et al., 2008]. These results indicate the potential of ES-DMA to quantify the surface density, configuration and binding energy of biological molecules and organic coatings on nanoparticles.

2.5 Quantum dots and nanoparticle conjugates

Quantum dots (QDs) are semiconducting nanoparticles or nanocrystals that exhibit quantum confinement and are useful in nanophotonics, advanced lighting and displays, as the next generation of photovoltaics (i.e. solar cells), and as dye replacements for molecular biology. Incident photons elevate electrons from the valence to the conduction band, leaving an excited electron-hole pair called an exciton. When the exciton is confined within a nanoparticle that is smaller than its Bohr radius, quantum confinement leads to increased separation between the valance and conduction bands with corresponding increases in the band gap and energy of the photon emitted upon recombination. Therefore, QD size is an essential feature because small changes in QD diameter lead to large changes in the energy of the emitted photon.

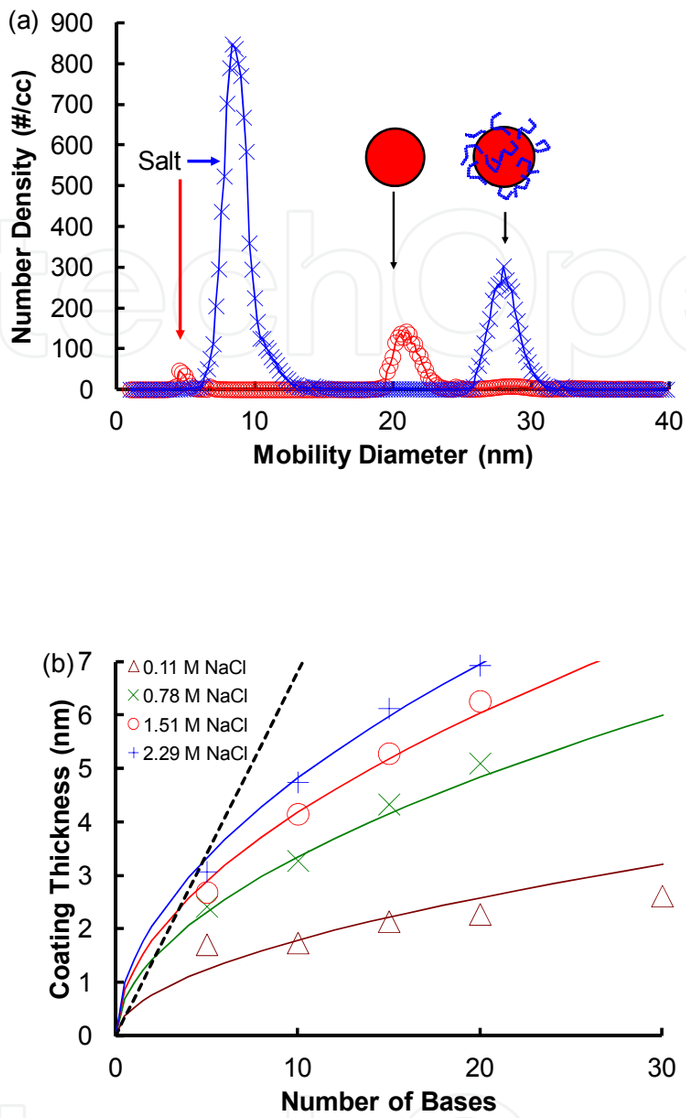

Fig. 8. (a) Size distributions of nominally 20 nm Au nanoparticles, one bare (O) and the other coated (x) with tethered single stranded DNA $(dT)_{20}$-SH. The difference between the two particle size distributions determines the apparent coating thickness. (b) Apparent coating thickness, H, versus number of dT nucleotides per strand, N_b, for a variety of salt concentrations, n_s. The dashed and solid lines respectively represent fits for a contour length model for fully stretched out DNA ($H \sim N_b$) versus that of a square root dependence ($H \sim N_b^{1/2}$) characteristic of strands coiled into low-grafting density layers (see text above). Reprinted with permission from [Pease et al., 2007]. Copyright (2011) American Chemical Society.

Figure 9a shows a typical ES-DMA size distribution of carboxylic acid terminated QDs, with peaks at 15.0 and 18.0 nm representing individual QDs and dimeric QD clusters. This size varies from that anticipated from optical measurements between 5 nm and 7 nm for several

reasons. First, these rod-shaped particles (see inset of Figure 9a) are coated with 40 kDa polyethylene glycol (PEG) and salt layers; the equivalent external size of an individual quantum dot without salt and polymer coatings is ~12.4 nm. Second, optical measurements (e.g., Figure 9b-d) reflect the size of the core for QDs with type I band alignment rather than the external size measured by ES-DMA. These differences indicate that optical, TEM, and ES-DMA measurements are mutually complementary for core-shell QDs: optical measurements ascertain the core, TEM gives the combined core and shell measurements, and ES-DMA provides core, shell and coating thicknesses.

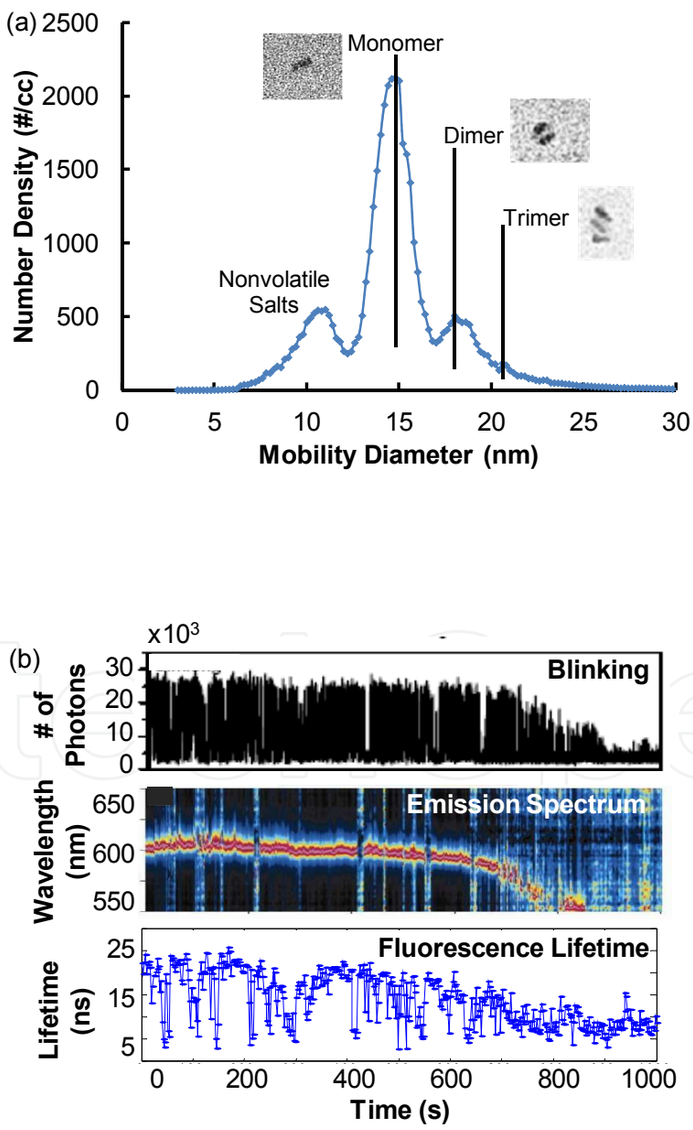

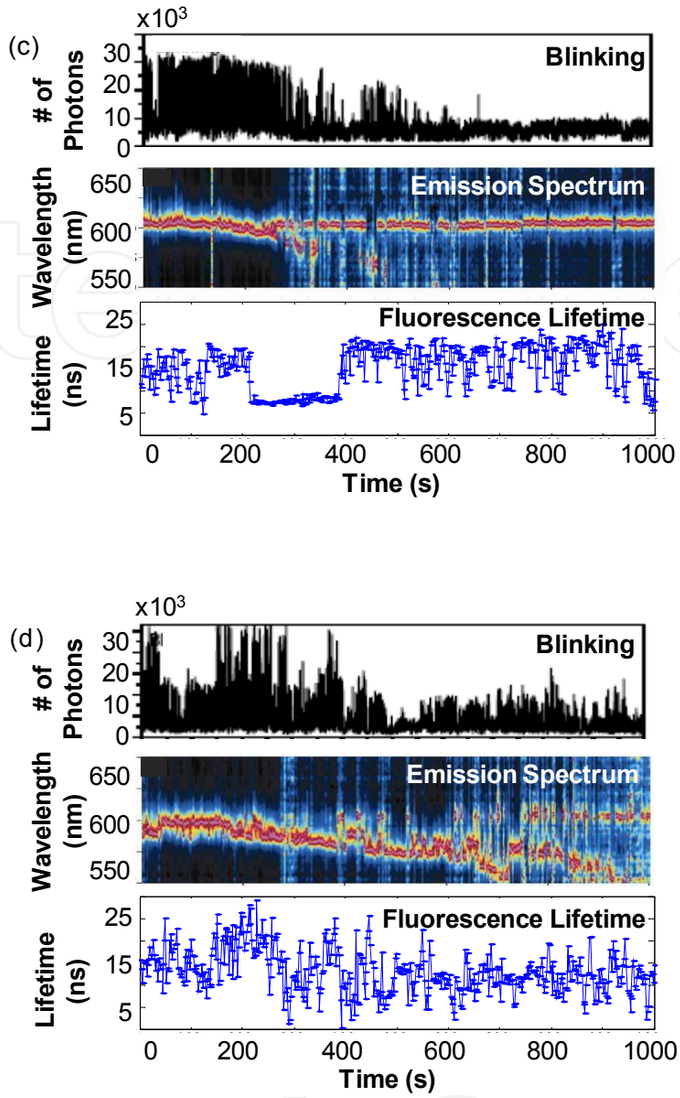

Fig. 9. (a) Raw ES-DMA size distribution of quantum dots at 0.4 μmol/L ($2.4 \cdot 10^{14}$ particles/mL) in 11 mmol/L acetic acid with insets representing TEM images of monomer, dimer and trimer. The first peak at ~11 nm is due to nonvolatile salts present in the original quantum dot solution. The intensity, spectrum, and lifetime of QD (b) monomeric, (c) dimeric, and (d) trimeric clusters

The ability to distinguish the soft and hard components indicates the potential to determine macromolecular conjugation. For example, Figure 10a compares QDs having a ZnS shell coated with mercaptoethanol (ME), ssDNA and double stranded DNA (dsDNA). ES-DMA reported an increase in the mobility diameter of the QDs complexes in the order of $d_{dsDNA} > d_{ssDNA} > d_{ME}$. This order is expected because mercaptoethanol is a shorter molecule than ssDNA, and dsDNA (persistence length ~50 nm) has a more extended conformation than ssDNA (persistence length ~1-3 nm). The extended conformation provides additional drag to the nanoparticle complex resulting in the larger apparent size measured. Similar detection

of macromolecular binding is seen in Figure 10b where dextran coated particles are conjugated with the lectins concanavalin (ConA) and wheat germ agglutinin (WGA). The conjugation clearly increased the apparent size of the nanoparticle complex.

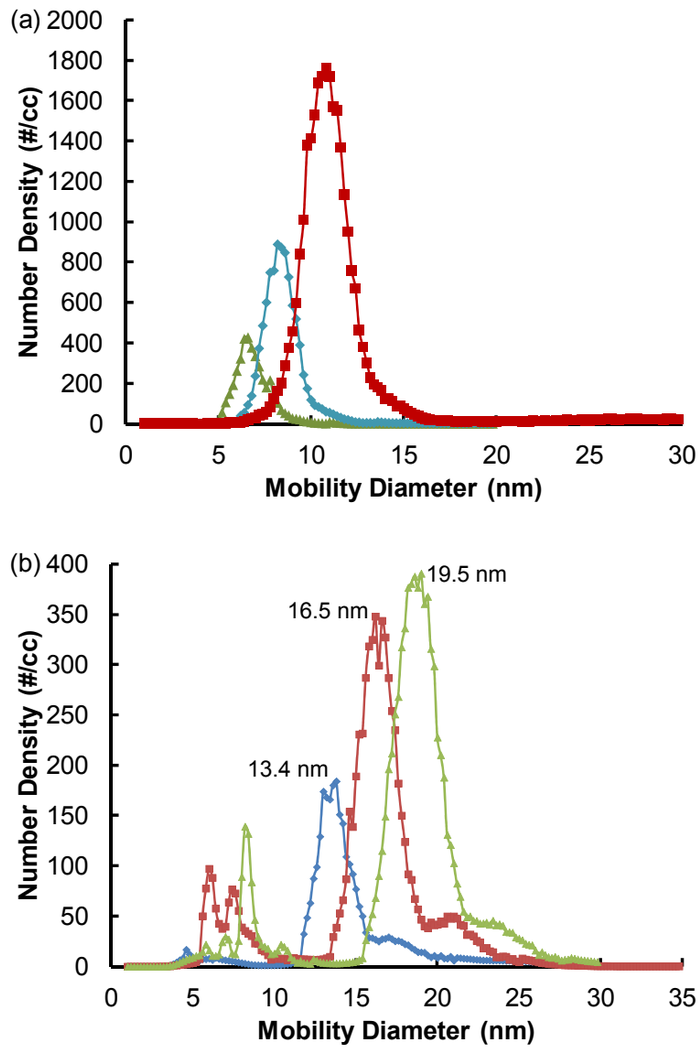

Fig. 10. ES-DMA size distributions of (a) QDs coated with mercaptoethanol (▲), ssDNA (♦), and dsDNA (■) and (b) dextran decorated bare nanoparticles bare (♦) or conjugated with WGA (■) or ConA (▲).

A further highlight of the use of ES-DMA to evaluate macromolecular conjugation is the effort of Yim, et al., to determine the number of QDs attached to genetically modified lambda phage [Yim et al., 2009]. Their biotinylated lambda phage present a rapid means of detecting harmful E. Coli bacteria because bacteriophages replicate much more rapidly than bacteria. Streptavidin coated QDs then bind to the biotinylated phage to provide colorimetric detection. The amount of bacteria is proportional to the amount of phage produced, and the signal from the assay is proportional to the average number of QDs bound to each phage. By comparing the conjugate size in ES-DMA size distributions with

that of individual QDs and the lambda phage, the number of QDs attached to the bacteriophage was determined using Eq. 5 by modeling the QD-phage conjugates as clusters of spheres (i.e., the phage) and rods (the streptaviding coated QDs) [Pease, 2011a]. More recently Tsai, et al., studied viral neutralization by quantifying antibody-virus binding [Tsai et al., 2011]. They compared the size of bare MS2 virus particles to those conjugated with anti-MS2 antibodies and reported an increase in the apparent size. They found that antibodies were responsible for formation of multiple virus complexes by acting as connectors between two virus particles (no dimerization was observed with the initial virus sample), indicating that ES-DMA is able to quantify viral aggregation as a form of virus neutralization. They then used their model to determine the stoichiometric ratio of bound antibodies to virus particles to find that infectivity strongly depends on binding stoichiometry not the type of antibody. Monoclonal and polyclonal antibodies both fell on a single infectivity versus stoichiometry curve.

2.6 Nanoparticles aggregates – Packing structure and kinetics

The development of structured materials for nanotechnology and nanobiotechnology requires readily available, rapid analytical techniques to determine the composition of nanostructured particles and clusters. ES-DMA is uniquely qualified to determine the packing and aerodynamic size of colloidal clusters in the nanometer range. For instance, aggregation of metallic nanoparticles may be detected via coupled plasmon resonances using UV-vis, however, this approach does not provide direct information on aggregate size and structure [Weisbecker et al., 1996]. Figure 11a shows an ES-DMA size distribution of multimers of gold nanoparticles with each multimer (e.g. dimers or trimers) appearing as a distinct peak separated by 2-3 nm. These multimers were prepared at the limit of colloidal stability by adding ammonium acetate buffer to a solution of gold nanoparticles to suppress electrostatic screening forces between like charged particles. Figure 11b shows how the ammonium acetate concentration induces aggregation in solution. Tsai, et al., followed the temporal kinetics of the nanoparticle aggregation in the liquid-phase using ES-DMA, as shown in Figure 11c [Tsai et al., 2008]. The monomer concentration decreases with the appearance of each higher order cluster (dimer, trimer, etc.) as anticipated from simple Brownian flocculation/aggregation. By fitting the data to a first principles kinetic model of the aggregation process, the surface charge on particles was extracted from the kinetic rate constants and found to be in good agreement with values reported in the literature (see Figure 11d).

ES-DMA can also be used to monitor protein aggregation. For example, Pease, et al., demonstrated that protein aggregates can be individually resolved and determined an equilibrium constant for the formation of dimers. This equilibrium constant was evaluated based on the number density, which can be obtained from the ES-DMA distribution [Pease et al., 2008]. Pease, et al., also demonstrated that ES-DMA can be used to characterize the size and packing structure of small clusters of identical nanoparticles in colloidal suspension [Pease et al., 2010a]. Essential to their analysis was the projected area model (Eq. 5) to calculate the cluster size, distinguishing collinear from close packed sphere arrangements without resorting to TEM. Several others used ES-DMA to analyze aggregates. For example, Lall, et al., used ES-DMA to determine the ultrafine aggregate surface area and volume distribution of silver aggregates [Lall et al., 2006a, 2006b]. This model is particularly apt for

very large aggregates comprising >10 particles/aggregate. Agglomeration of silver nanoparticles was also reported by Elzey & Grassian using ES-DMA [Elzey & Grassian, 2010]. They investigated agglomeration as a function of pH, which determines the dissolution of silver ions in aqueous environments.

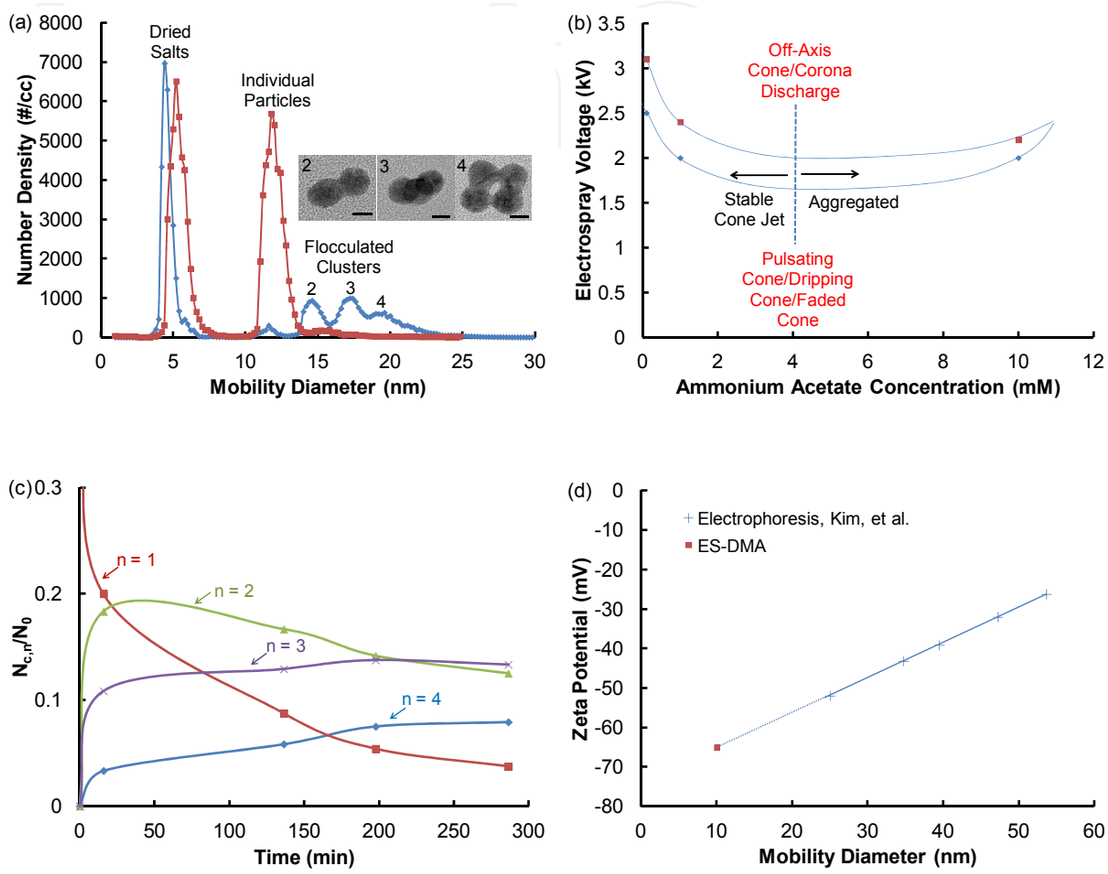

Fig. 11. (a) Size distribution of multimers of gold nanoparticles. The inset shows the TEM images of dimers, trimers, etc. (b) Onset of gold nanoparticle aggregation as a function of ammonium acetate buffer concentration. (c) Normalized concentration of aggregates vs reaction time at an ammonium acetate concentration of 7.89 mmol/L. (d) Relation between surface potential and particle diameter for gold nanoparticles as measured by ES-DMA (■) and reported in the literature (+). The absolute value from ES-DMA was 65 mV. Panel c reprinted with permission from [Tsai et al., 2008]. Copyright (2008) American Chemical Society.

2.7 Optimizing cluster production and purity

Though most ES-DMA research centers on analytical scale characterization, this technique also holds potential as a preparative scale purification tool. For example, ES-DMA separates two particle clusters (dimers) from three particle clusters (trimers), and Kang, et al., have shown that cluster composition may affect cluster photonic properties such as the

wavelength evolution, intensity, blinking and radiative lifetime [Kang et al., 2012] (see Figures 9b, 9c, and 9d). To enhance the yield and purity (i.e., how many nominally three-particle clusters actually contain three particles), Pease modeled the ES-DMA technique as a function of nanoparticle properties (size, concentration, etc.) using Monte Carlo simulations [Pease, 2011a]. Figure 12a shows that tuning the initial solution concentration of nanoparticles optimizes the yield of each kind of cluster. The concentration of dimers and subsequently trimers begins to increase as the fraction of monomers declines. Figure 12a also shows that at a concentration of ~$7.0 \cdot 10^{14}$ particles/mL, only 5% of the particles/strands in the size distribution are not monomers providing a sensitive metric for the onset of aggregation. Around 10^{15} particles/mL the concentrations of monomer, dimer, trimer, and higher order clusters all approach parity.

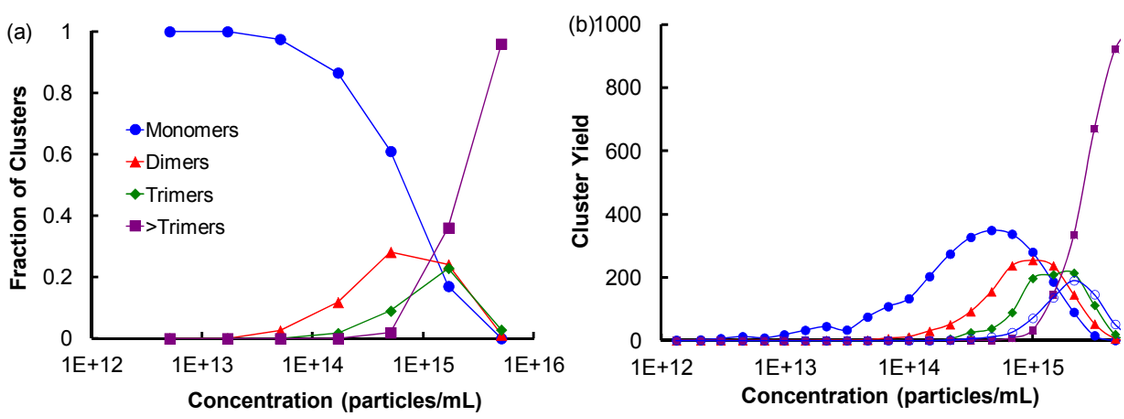

Fig. 12. (a) Monte Carlo simulation using 1000 droplets each exactly 150 nm in diameter for solution concentrations ranging from 10^{12} to 10^{16} particles/mL. (b) The yield for monomers (filled circles), dimers (filled triangles), trimers (filled diamonds), tetramers (open circles), and clusters composed of five or more particles, as a function of initial solution concentration.

To determine the cluster purity, the size distribution of heterogeneously sized particles must be calculated. There are two options for determining the average mobility diameter, d_{ave}. The first option as outlined in Pease, et al., calculates the three projected areas, A_i, orthogonal to the cluster's principle axes (see Figure 13) as given in Eqs. 5 and 6 [Pease et al., 2007]. The area of each projection may be determining from the center-to-center distances, h_i, between the circles in that projection as given by

$$A_1 = \pi/4(d_1^2 + d_2^2 + d_3^2)$$
$$A_2 = \pi/4(d_1^2 + d_3^2) - A_{ov}(h_1)$$
$$A_3 = A_1 - A_{ov}(h_2) - A_{ov}(h_3), \quad (6)$$

where d_1, d_2, and d_3 are the diameters of 3 clusters and $d_1 \geq d_2 \geq d_3$ [Pease, 2011a].

The second option is to employ the proportionality constants determined previously by Pease, et al., for homogeneous clusters [Pease et al., 2010a]. They show that $d_{ave} = kd_p$, where k is the proportionality with values of 1.526, 1.724, and 1.875 for close packed trimers, tetramers, and pentamers, respectively. For heterogeneously sized particles, $d_{ave} = \sum_{i=1}^{n} d_i / n$. Overlaps in the size distribution (see Figure 12b) increase the probability that particles of neighboring size will contaminate each other, decreasing the purity of selected clusters. Pease found that and when the coefficient of variation is <13%, this overlap in the size distributions is not significant. In more recent work, Li, et al., also investigated the formation of clusters during the electrospray process [Li et al., 2011]. They developed a statistical model to determine the extent of ES droplet induced aggregation and how it alters the results.

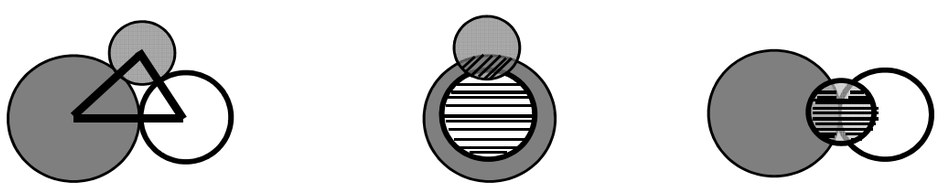

Fig. 13. Depiction of the three projected areas, A_i, used to determine the mobility of a close packed trimeric cluster. Crosshatching in the second and third geometries represent overlap area, A_{ov}.

3. Comparison of ES-DMA to similar techniques

Each of the above examples highlights the potential of ES-DMA to analyze nanoparticles. The remainder of this section compares this powerful technique to generally available classes of techniques commonly used to characterize nanomaterials such as electron microscopy and light scattering.

3.1 Electron microscopy

EM techniques such as transmission electron microscopy (TEM) and scanning electron microscopy (SEM) are direct methods to characterize nanoparticles with subnanometer resolution. EM methods provide compelling images that provide unbiased insight into the *actual* geometry and structure of electro-opaque particles, especially for the hard portions of bionanoparticles as described above. Crystallinity of the particles can also be investigated by generating diffraction patterns using EM. Despite providing very high resolution and beautiful images, EM methods remain expensive to install and operate. To rigorously determine the average nanoparticle size, several hundred to thousands of nanoparticles must be measured [Tsai et al., 2008a, 2008b], which is time consuming (of the order of days to weeks) without automation that is not widely available. For less homogeneous systems or soft materials, multimodal distributions and electron beam damage present further challenges to rigorous TEM measurement. Pease, et al., compared TEM with ES-DMA for

quantitative characterization of virus particles and concluded that ES-DMA has a greater rapidity (millions of particles per hr compared to thousands of particles per hour) and statistical significance than TEM [Pease et al., 2009a, 2010b, 2011].

3.2 Light scattering techniques

Light scattering techniques such as multiangle light scattering (MALS) and dynamic light scattering (DLS) measure the intensity fluctuations of scattered light in solution. As light is focused using a laser on the particles moving due to Brownian motion, measured photon intensity fluctuates, from which the z-average hydrodynamic diameter may be estimated. The z-average molecular weight typically exceeds the mass average molecular weight for the most common distributions. In contrast, ES-DMA measures the number average diameter. Otherwise, light scattering and ES-DMA techniques are similar in that they are rapid, inexpensive, and produce statistical significant averages. Though the suspending medium of the sample influences the DLS measurements, it may be preferable for dirty samples minimizing the preparation time required for sample clean up. When characterizing structures with high aspect ratios (e.g., carbon nanotubes), MALS and DLS produce ensemble-average lengths of broad distributions using root-mean square length metrics assuming the nanotubes to have monomodal length distributions [Bauer et al., 2008; Chun et al., 2008; Hinds, 1999]. In contrast ES-DMA measures the size of each nanotube individually to assemble the full multimodal length distributions [Pease et al., 2009b]. Also, DLS does not directly correlate the size or number of individual particles with the size of an aggregate and cannot resolve individual aggregate concentrations within multimodal distributions. Clearly distinguishing clusters differing by only a single particle remains challenging, especially for particles less than 30 nm [Nguyent & Flagan, 1991; Nie et al., 2006].

3.3 Statistical comparison with different techniques

Perhaps the most comprehensive comparison of the primary techniques available to analyze nanoparticle size was performed at NIST on gold nanoparticles. Table 1 shows the statistical data comparison of mean diameters of gold nanoparticles using at least 7 different techniques. Though all the values are in reasonable agreement, some uncertainty is to be expected even from well calibrated systems. Several other authors have compared techniques including MALS, DLS, AFFFF, EM, and ES-DMA using organic (e.g., viruses and virus like particles) and inorganic (carbon nanotubes) nanomaterials [Lute et al., 2008; Pease et al., 2008, 2009a, 2009b]. For example, Lute, et al., and Pease, et al., both found ES-DMA measurements of viruses and virus like particles to be smaller than those of AFFFF-MALS. Reasons for the difference include the following. ES-DMA measures the external size of the virus particle, whereas AFFFF-MALS reports the radius of gyration that depends on the mass distribution of the particle. Also, ES-DMA measures the dry particle size in contrast to the light scattering techniques and AFFFF that measure particles in solution [Pease et al., 2008]. Organic particles are more likely to experience favorable enthaplic interactions in water rich environments that increase their hydrodynamic radius. In dry environments TEM and ES-DMA report similar averages for sufficiently large sample sizes [Lute et al., 2008; Pease, 2012]. Pease, et al., also report analysis of the length distribution of carbon nanotubes

using several techniques including AFM, MALS, DLS, and FFF. Here hydrophilic interactions exert little to no influence on the size of the particle and each of these techniques reports similar results [Pease et al., 2009b]. Most recently, Kapelios, et al., characterized the size and molecular mass of proteins and complexes, comparing ES-DMA with light scattering techniques, multi-angle laser light scattering (MALLS) and quasi-elastic light scattering (QELS) [Kapelios et al., 2011]. Similar to Pease, et al., they found that ES-DMA measurements are smaller than those of MALLS and QELS, as expected for proteinacious materials.

Technique	Analyte form	Size of nominally 10 nm particles (nm)	Size of nominally 30 nm particles (nm)	Size of nominally 60 nm particles (nm)
ES-DMA	Dry, aerosol	11.3±0.1	28.4±1.1	56.3±1.5
TEM	Dry, on substrate	8.9±0.1	27.6±2.1	56.0±0.5
DLS (a)	Diluted liquid suspension	13.5±0.1	28.6±0.9	56.6±1.4
DLS (b)	Diluted liquid suspension	13.5±0.1	26.5±3.6	55.3±8.3
AFM	Dry, on substrate	8.5±0.3	24.9±1.1	55.4±0.3
SEM	Dry, on substrate	9.9±0.1	26.9±0.1	54.9±0.4
SAXS	Native liquid suspension	9.1±1.8	24.9±1.2	53.2±5.3

Table 1. Mean diameter and expanded uncertainty average particle diameter of gold nanoparticles [adapted from, NIST certificate, 2007]. DLS results: (a) 173° scattering angle, (b) 90° scattering angle. The uncertainties represent repeatability not the width of the particle size distributions.

4. Future of ES-DMA

In summary, ES-DMA is a powerful tool to characterize and fabricate nanoparticles. Several nanoparticle systems have been characterized using ES-DMA, including quantum dots, linear polymers, and complex colloidal nanomaterials. However, a major growth area for this technique is likely to be in the analysis of soft complex nanomaterials. For example. ES-DMA has significant potential to characterize biochemical reactions including those that assay for nano-therapeutics and bio-pharmaceuticals. Indeed, real-time detection of biological reactions is one of the most promising emerging applications of this instrument. ES-DMA is well suited for this future given its dynamic operating range from 150 Da up to 10^{11} Da. The lower limit of detection is still under refinement with significant improvements underway using high precision home-built DMAs that employ funnel shaped flow injectors to delay the onset of the turbulence. These systems boast sub-angtrom precision on the molecule's mobility diameter [Eichler et al., 1998; Fernandez de la Mora, 2011; Hollertz et al., 2011]. ES-DMA is also well suited to evaluate the role of aggregation, which may be particularly advantageous for detecting protein aggregates in biomanufacturing environments. However, to realize its full potential, further exploration and excellent coordination between biologists, chemists and engineers is required to expand the boundaries of ES-DMA.

5. Acknowledgements

We express appreciation for helpful conversations with De-Hao Tsai, Michael R. Zachariah and Michael J. Tarlov. We sincerely appreciate Hedieh Saffari, Joshua Gustafson, and Hamid Ghandehari for their help with biological particle systems. We thank Silvia De Paoli Lacerda, HyeongGon Kang, Peter Yim, Jeremy I. Feldblyum, Jeeseong Hwang, Matthew L. Clarke, and Phillip Deshong for the nanoparticle samples and conjugate data.

6. References

Adamuti-Trache, M.; McMullen, W. E. & Douglas, J. F. (1996). Segmental Concentration Profiles of End-Tethered Polymers with Excluded-Volume and Surface Interactions. *J. Chem. Phys.* Vol. 105, No. 11 (September 1996), pp. 4798-4811.

Allen, M. D. & Raabe, O. G. (1985). Slip Correction Measurements of Spherical Solid Aerosol Particles in an Improved Millikan Apparatus. *Aerosol Sci. Technol.*. Vol. 4, No. 3 (1985), pp. 269-286.

Anumolu, R.; Gustafson, J. A.; Magda, J. J.; Cappello, J.; Ghandehari, H. & Pease III, L. F. (2011) Fabrication of Highly Uniform Nanoparticles from Recombinant Silk-Elastinlike Protein Polymers for Therapeutic Agent Delivery. *ACS Nano*. Vol. 5, No. 7, (July 2011), pp. 5374-5382.

Attri, A. K. & Minton, A. P. (2005). New Methods for Measuring Macromolecular Interactions in Solution via Static Light Scattering: Basic Methodology, and Application to Non-Associating and Self-Associating Proteins. *Anal. Biochem.* Vol. 337, No. 1 (February 2005), pp. 103–110.

Bacher, G.; Szymanski, W. W.; Kaufman, S. L.; Zollner, P.; Blaas, D. & Allmaier, G. (2001). Charge-Reduced Nano Electrospray Ionization Combined with Differential Mobility Analysis of Peptides, Proteins, Glycoproteins, Noncovalent Protein Complexes and Viruses. *J. Mass Spectrom*. Vol. 36, No. 9, (September 2001), pp. 1038-1052.

Baron, P.A.; Deye, G. J. & Fernback, J. (1994). Length Separation of Fibers. *Aerosol Sci. Technol.* Vol. 21, No. 2, (1994), pp. 179–192.

Barry, C. R.; Steward, M. G.; Lwin, N. Z. & Jacobs, H. O. (2003). Printing Nanoparticles from the Liquid and Gas Phases Using Nanoxerography. *Nanotechnology*. Vol. 14, No. 10, (August 2003), pp. 1057-1063.

Barry, C. R.; Lwin, N. Z.; Zheng, W. & Jacobs, H. O. (2003). Printing Nanoparticle Building Blocks from the Gas Phase Using Nanoxerography. *Appl. Phys. Lett*. Vol. 83, No. 26, (October 2003), pp. 5527-5529.

Bauer, B. J.; Fagan, J. A.; Hobbie, E. K.; Chun, J. & Bajpai, V. (2008). Chromatographic Fractionation of SWNT/DNA Dispersions with On-Line Multi-Angle Light Scattering. *J. Phys. Chem. C.* Vol. 112, No. 6, (January 2008), pp. 1842-1850.

Benson, S. D.; Bamford, J. K.; Bamford, D. H. & Burnett., R. M. (2002). The X-ray Crystal Structure of P3, the Major Coat Protein of the Lipid-Containing Bacteriophage PRD1, at 1.65 A° Resolution. *Acta Crystallogr., Sect D: Biol. Crystallogr.* Vol. 58, No. 1, (January 2002), pp. 39–59.

Bondos, S. E. (2006). Methods for Measuring Protein Aggregation. *Curr. Anal. Chem*. Vol. 2, No. 2, (April 2006), pp. 157–170, ISSN: 1573-4110.

Casper, L. D. & Klug, A. (1962) Physical Principles in the Construction of Regular Viruses. *Cold Spring Harbor Symp. Quant. Biol.* Vol. 27, (1962), pp. 1–24.

Chen, B. T.; Yeh, H. C. & Hobbs, C. H. (1993). Size Classification of Carbon Fiber Aerosols. *Aerosol Sci. Technol.*, Vol. 19, No. 2, (August 1993), pp. 109–120.

Cole, K. D.; Pease III, L. F.; Tsai, D. H.; Singh, T.; Lute, S.; Brorson, K. A. & Wang, L. (2009). Particle Concentration Measurement of Virus Samples Using Electrospray Differential Mobility Analysis and Quantitative Amino Acid Analysis. *J. Chromatogr. A*. Vol. 1216, No. 30, (July 2009), pp. 5715–5722.

Chang, T. H.; Cheng, C. P. & Yeh, C. T. (1992). Deuterium Nuclear Magnetic Resonance Characterization of Particle Size Effect in Supported Rhodium Catalysts. *J. Catal.* Vol. 138, No. 2, (December 1992), pp. 457-462.

Chun, J.; Fagan, J. A.; Hobbie, E. K. & Bauer, B. (2008). Size Separation of Single-Wall Carbon Nanotubes by Flow-Field Flow Fractionation. *J. Anal. Chem*. Vol. 80, No. 7, (February 2008), pp. 2514-2523.

Colter, J. S. & Ellem, K. A. O. (1961). Structure of Viruses. *Annu. Rev. Microbiol.* Vol. 15, (October 1961), pp. 219–244.

Dai, Q.; Liu, X.; Coutts, J.; Austin, L. & Huo, Q. (2008). A One-Step Highly Sensitive Method for DNA Detection Using Dynamic Light Scattering. *J. Am. Chem. Soc.* Vol. 130, No. 26, (June 2008), pp. 8138-8139.

Deye, G. J.; Gao, P.; Baron, P. A. & Fernback, J. (1999). Performance Evaluation of a Fiber Length Classifier. *Aerosol Sci. Technol.* Vol. 30, No. 5, (1999), pp. 420–437.

Dixkens, J. & Fissan, H. (1999). Development of an Electrostatic Precipitator for Off-Line Particle Analysis. *Aerosol Sci. Technol.* Vol. 30, No. 5, (1999), pp. 438-453.

Eichler, T.; Juan, L. D. & Fernandez de la Mora, J. (1998). Improvement of the Resolution of TSI's 3071 DMA via Redesigned Sheath air and aerosol inlets. *Aerosol Sci. Technol.* Vol. 29, No. 1, (1998), pp. 39–49.

Elzey, S. & Grassian, V. H. (2010). Agglomeration, Isolation and Dissolution of Commercially Manufactured Silver Nanoparticles in Aqueous Environments. *J. Nanopart. Res.* Vol. 12, No. 5, (2010), pp. 1945-1958.

Epstein, P. S. (1924). On the Resistance Experienced by Spheres in their Motion through Gases. *Phys. Rev.* Vol. 23, No. 6, (1924), pp. 710-733.

Fernandez de la Mora, J. (2011). Electrical Classification and Condensation Detection of Sub-3 nm Aerosols, In: *Aerosol Measurement: Principles, Techniques, and Applications* (3rd edition), Baron, P.A.; Kulkarni, P. & Willeke, K., pp. 607-721, John Wiley & Sons, Inc., ISBN 978-0-470-38741-2, New York, USA.

Fissan, H. J.; Helsper, C. & Thielen, H. J. (1983). Determination of Particle-Size Distributions by Means of an Electrostatic Classifier. *J. Aerosol Sci.* Vol. 14, No. 3, (1983), pp. 354-357.

Fissan, H.; Kennedy, M. K.; Krinke, T. J. & Kruis, F. E. (2003). Nanoparticles from the Gas phase as Building Blocks for Electrical Devices. *J. Nanopart Res.* Vol. 5, No. 3-4, (August 2003), pp. 299-310.

Fuchs, N. A. (1963). On the Stationary Charge Distribution on Aerosol Particles in a Bipolar Ionic Atmosphere. *Pure Appl. Geophys.* Vol. 56, No. 1, (1963), pp. 185-193.

Hinds, W. C. (January 1999). *Aerosol Technology: Properties, Behavior, and Measurement of Airborne Particles* (2nd edition), John-Wiley & Sons, Inc., ISBN 978-0-471-19410-1, New York, USA.

Hogan, C. J.; Kettleson, E. M.; Ramaswami, B.; Chen, D. R. & Biswas, P. (2006). Charge Reduced Electrospray Size Spectrometry of Mega- and Gigadalton Complexes: Whole Viruses and Virus Fragments. *Anal. Chem.* Vol. 78, No. 3, (February 2006), pp. 844–852.

Hogan, C. J.; Yun, K. M.; Chen, D. R.; Lenggoro, I. W.; Biswas, P.; Okuyama, K. (2007) Controlled Size Polymer Particle Production via Electrohydrodynamic Atomization. *Colloids Surf., A: Physicochem. Eng. Aspects.* Vol. 311, No. 1-3, (December 2007), pp. 67-76.

Hogan, C. J. & Biswas, P. (2008). Monte Carlo Simulation of Macromolecular Ionization by Nanoelectrospray. *J. Am. Soc. Mass Spectrom.* Vol. 19, No. 8, (August 2008), pp. 1098–1107.

Hollertz, M.; Elliott, J. T.; Lewis, J.; Mansfield, E. R.; Whetten, W. D.; Knotts IV, T. A.; Tarlov, M. J.; Zachariah, M. R. & Pease III, L. F. (2011). Structural Differentiation of Oxytocin in Cyclical and Linear Conformations Using High Resolution Differential Mobility Analysis. *Anal. Chem.* (2011), submitted.

Hung, L. H. & Lee, A. P. (2007). Microfluidic Devices for the Synthesis of Nanoparticles and Biomaterials. *J. Med. Biol. Eng*. Vol. 27, No. 1, (2007), pp. 1-6.

Jacobs, H. O.; Campbell, S. A. & Steward, M. G. (2002). Approaching Nanoxerography: The Use of Electrostatic Forces to Position Nanoparticles with 100 nm Scale Resolution. *Adv. Mater.* 2002, Vol. 14, No. 21, (November 2002), pp. 1553-1557.

Johnson, B. K. & Prud'homme, R. K. (2003). Mechanism for Rapid Self-Assembly of Block Copolymer Nanoparticles. *Phys. Rev. Lett.* Vol. 91, No. 11, (2003), pp. 118302-1-118302-4.

Juan, L. D. & Fernandez de la Mora, J. (March 1996). On-line Sizing of Colloidal Nanoparticles via Electrospray and Aerosol Techniques, In: *Nanotechnology*: Molecularly Designed Materials, (Vol. 622), Chow, G. M. & Gonsalves, K. E., pp. 20-41, ACS Publications, ISBN13: 9780841233928

Kang, H.; Clarke, M. L.; Pease III, L. F.; DePaoli Lacaerda, S. H.; Karim, A. & Hwang, J. (2011). Analysis of the Optical Properties of Clustered Colloidal Quantum Dots by the Chi-Square Distribution of the Fluorescence Lifetime Curves, *ASC Nano* (2011) manuscript.

Kang, H.; Clarke, M. L.; DePaoli Lacaerda, S. H.; Pease III, L. F. & Hwang, J. (2012). Multimodal Optical Studies of Single and Clustered Colloidal Quantum Dots Towards the Long-term Performance Evaluation of Optical Properties of Quantum Dot-included Molecular Imaging Phantoms. *Biomed. Opt. Express* (2012), submitted.

Kapellios, S.; Karamanou, M. F.; Sardis, M.; Aivaliotis, A.; Economou, S. & Pergantis, A. (2011). Using Nanoelectrospray Ion Mobility Spectrometry (GEMMA) to Determine the Size and Relative Molecular Mass of Proteins and Protein Assemblies: A

Comparison with MALLS and QELS. *Anal. Bioanal. Chem*. Vol. 399, No. 7, (March 2011), pp. 2421-2433.

Kim, S. H. & Zachariah, M. R. (2005). In-Flight Size Classification of Carbon Nanotubes by Gas Phase Electrophoresis. *Nanotechnology*. Vol. 16, No. 10, (August 2005), pp. 2149–2152.

Kim, S. H. & Zachariah, M. R. (2006). In-Flight Kinetic Measurements of the Aerosol Growth of Carbon Nanotubes by Electrical Mobility Classification. *J. Phys. Chem. B*. Vol. 110, No. 10, (February 2006), pp. 4555–4562.

Kim, S. H. & Zachariah, M. R. (2007a). Gas-Phase Growth of Diameter-Controlled Carbon Nanotubes. *Mater. Lett.* Vol. 61, No. 10, (April 2007), pp. 2079-2083.

Kim, S. H. & Zachariah, M. R. (2007b). Understanding Ion-Mobility and Transport Properties of Aerosol Nanowires. *J. Aerosol Sci*. Vol. 38, No. 8, (August 2007), pp. 823-842.

Kim, S. K.; Ha, T. & Schermann, J. P. (2010). Advances in Mass Spectrometry for Biological Science. *Phys. Chem. Chem. Phys.* Vol. 12, No. 41, (November 2010), pp. 13366–13367.

Knapman, T. W.; Morton, V. L.; Stonehouse, N. J.; Stockley, P. G. & Ashcroft., A. E. (2010). Determining the Topology of Virus Assembly Intermediates Using Ion Mobility Spectrometry-Mass Spectrometry. *Rapid Commun. Mass Spectrom.* Vol. 24, No. 20, (October 2010), pp. 3033–42.

Knutson, E. O. & Whitby, K. T. (1975). Aerosol Classification by Electric Mobility: Apparatus, Theory, and Applications. *J. Aerosol Sci*. Vol. 6, No.6, (November 1975), pp. 443-451.

Krinke, T. J.; Deppert, K.; Magnusson, M. H. & Fissan, H. (2002). Nanostructured Deposition of Nanoparticles from the Gas Phase. *Part. Part. Syst. Char.* Vol. 19, No. 5, (November 2002), pp. 321-326.

Krinke, T. J.; Fissan, H. & Deppert, K. (2003). Deposition of Aerosol Nanoparticles on Flat Substrate Surfaces. *Phase Transitions.* Vol. 76, No. 4-5, (May 2003), pp. 333-345.

Kuzmanovic, D. A.; Elashvili, I.; O'Connell, C. & Krueger, S. (2008). A Novel Application of Small-Angle Scattering Techniques: Quality Assurance Testing of Virus Quantification Technology. *Radiat. Phys. Chem.* Vol. 77, No. 3, (March 2008), pp. 215–224.

Lall, A. A. & Friedlander, S. K. (2006). On-Line Measurement of Ultrafine Aggregate Surface Area and Volume Distributions by Electrical Mobility Analysis: I. Theoretical Analysis. *J. Aerosol Sci.* Vol. 37, No. 3, (March 2006), pp. 260-271.

Lall, A. A. & Friedlander, S. K. (2006). On-Line Measurement of Ultrafine Aggregate Surface Area and Volume Distributions by Electrical Mobility Analysis: II. Comparison of Measurements and Theory. *J. Aerosol Sci.* Vol. 37, No. 3, (March 2006), pp. 272-282.

Lenggoro, I. W.; Xia, B. & Okuyama, K. (2002). Sizing of Colloidal Nanoparticles by Electrospray and Differential Mobility Analyzer Methods. *Langmuir*. Vol. 18, No. 12, (May 2002), pp. 4584–4591.

Lenggoro, I. W.; Widiyandari, H.; Hogan Jr., C. J.; Biswas, P. & Okuyama, K. (2007). Colloidal Nanoparticle Analysis by Nanoelectrospray Size Spectrometry with a Heated Flow. *Anal. Chim. Acta.* Vol. 585, No. 2, (March 2007), pp. 193-201.

Li, M.; Guha, S.; Zangmeister, R. A.; Tarlov, M. J. & Zachariah, M. R. (2011). Quantification and Compensation of Nonspecific Analyte Aggregation in Electrospray Sampling. *Aerosol Sci. Technol.*. Vol. 45, No.7, (March 2011), pp. 849-860.

Loo, J. A.; Berhane, B.; Kaddis, C. S.; Wooding, K. M.; Xie, Y. M.; Kaufman, S. L. & Chernushevich, I. V. (2005). Electrospray Ionization Mass Spectrometry and Ion Mobility Analysis of the 20S Proteasome Complex. *J. Am. Soc. Mass Spectrom.* Vol. 16, No. 7, (July 2005), pp. 998-1008.

Lute, S.; Riordan, W.; Pease III, L. F.; Tsai, D. H.; Levy, R.; Haque, M.; Martin, J.; Moroe, I.; Sato, T.; Morgan, M.; Krishnan, M.; Campbell, J.; Genest, P.; Dolan, S.; Tarrach, K.; Meyer, A.; the PDA Virus Filter Task Force; Zachariah, M. R.; Tarlov, M. J.; Etzel, M. & Brorson, K. (2008). A Consensus Rating Method for Small Virus-Retentive Filters. I. Method Development. *PDA J. Pharm. Sci. Technol.* Vol. 62, No. 5, (October 2008), pp. 318–333.

Moisala, A.; Nasibulin, A. G.; Shandakov, S. D.; Jiang, H. & Kauppinen, E. I. (2005). On-line Detection of Single-Walled Carbon Nanotube Formation During Aerosol Synthesis Methods. *Carbon.* Vol. 43, No. 10, (August 2005), pp. 2066-2074.

Netz, R. R. & Andelman, D. (2003). Neutral and Charged Polymers at Interfaces. *Phys. Rep.* Vol. 380, No. 1-2, (June 2003), pp. 1-95.

Nguyent, H. V. & Flagan, R. C. (1991). Particle Formation and Growth in Single-Stage Aerosol Reactors. *Langmuir*. Vol. 7, No. 8, (August 1991), pp. 1807-1814.

Nie, Z.; Xu, S.; Seo, M.; Lewis, P. C. & Kumacheva, E. (2005). Polymer Particles with Various Shapes and Morphologies Produced in Continuous Microfluidic Reactors. *J. Am. Chem. Soc.* Vol. 127, No. 22, (May 2005), pp. 8058-8063.

Nie, Z. X.; Tzeng, Y. K.; Chang, H. C.; Chiu, C. C.; Chang, C. Y.; Chang, C. M. & Tao, M. H. (2006). Microscopy-Based Mass Measurement of a Single Whole Virus in a Cylindrical Ion Trap. *Angew. Chem. Int. Ed. Engl.* 2006, Vol. 45, No. 48, (December 2006), pp. 8131-8134.

NIST Certificate (2007). *Nanoparticle Standards at NIST: Gold Nanoparticle Reference Materials*.http://www.mel.nist.gov/tripdf/NIST/05_Hackley%20TNW%20AuRM%20talk%2002.05.08.VAH_final.pdf (2007).

Park, J. Y. & Phaneuf, R. J. (2003) Investigation of the Direct Electromigration Term for Al Nanodots within the Depletion Zone of a pn Junction. *J. Appl. Phys.* Vol. 94, No. 10, (2003), pp. 6883-6886.

Pease III, L. F.; Tsai, D. H.; Zangmeister, R. A.; Zachariah, M. R. & Tarlov, M. J. (2007). Quantifying the Surface Coverage of Conjugated Molecules on Functionalized Nanoparticles. *J. Phys. Chem. C.* Vol. 111, No. 46, (November 2007), pp. 17155-17157.

Pease III, L.F.; Elliott, J. T.; Tsai, D. H.; Zachariah, M. R. & Tarlov, M. J. (2008) Determination of Protein Aggregation with Differential Mobility Analysis: Application to IgG Antibody. *Biotechnol. Bioeng.* Vol. 101, No. 6, (December 2008), pp. 1214–1222.

Pease III, L. F.; Lipin, D. I.; Tsai, D. H.; Zachariah, M. R.; Lua, L. H. L.; Tarlov, M. J. & Middelberg, A. P. J. (2009a). Quantitative Characterization of Virus-like Particles by Asymmetrical Flow Field Flow Fractionation, Electrospray Differential Mobility Analysis, and Transmission Electron Microscopy. *Biotechnol. Bioeng.* Vol. 102, No. 3, (February 2009), pp. 845-855.

Pease III, L.F.; Tsai, D. H.; Fagan, J. A.; Bauer, B. J.; Zangmeister, R. A.; Tarlov, M. J. & Zachariah, M. R. (2009b). Length Distributions of Single Wall Carbon Nanotubes in Aqueous Suspensions Measured by Electrospray-Differential Mobility Analysis. *Small.* Vol. 5, No. 24, (December 2009), pp. 2894-2901.

Pease III, L. F.; Tsai, D.-H.; Zangmeister, R. A.; Hertz, J. L.; Zachariah, M. R. & Tarlov, M. J. (2010a). Packing and Size Determination of Colloidal Nanoclusters. *Langmuir*. Vol. 26, No. 13, (May 2010), pp. 11384–11390.

Pease III, L. F.; Feldblyum, J. I.; DePaoli Lacerda, S. H.; Liu, Y.; Hight-Walker, A.; Anumolu, R.; Yim, P. B.; Clarke, M. L.; Kang, H. G. & Hwang, J. (2010b). Structural Analysis of Soft Multicomponent Nanoparticle Clusters. *ACS Nano.* Vol. 4, No. 11, (November 2010), pp. 6982-6988.

Pease III, L. F.; Sorci, M.; Guha, S.; Tsai, D. H.; Zachariah, M. R.; Tarlov, M. J. & Belfort, G. (2010c). Probing the Nucleus Model for Oligomer Formation During Insulin Amyloid Fibrillogenesis. *Biophys. J.* Vol. 99, No. 12, (December 2010), pp. 3979-85.

Pease III, L. F.; Tsai, D. H.; Zangmeister, R. A.; Zachariah, M. R. & Tarlov, M. J. (2010d). Analysis of Gold Nanoparticles by Electrospray Differential Mobility Analysis (ES-DMA). NIST-NCL Joint Assay Protocol, PCC-10, Version 1.1.

Pease III, L. F.; Tsai, D. H.; Brorson, K. A.; Guha, S.; Zachariah, M. R.; & Tarlov, M. J. (2011). Physical Characterization of Viral Ultra Structure, Stability, and Integrity. *Anal. Chem.* Vol. 83, No. 5, (February 2011), pp. 1753-1759.

Pease III, L. F. (2011a). Optimizing the Yield and Selectivity of High Purity Nanoparticle Clusters. *J. Nanopart. Res.* Vol. 13, No. 5, (2011), 2157-2172.

Pease III, L.F. (2012). Physical Analysis of Virus Particles. *Trends Biotechnol.* (2012), in press, DOI: 10.1016/j.tibtech.2011.11.004.

Rader, D. J. (1990). Momentum Slip Correction Factor for Small Particles in Nine Common Gases. *J. Aerosol Sci*. Vol. 21, No. 2, (1990), pp. 161-168.

Regenmortel, M. H. V.; Fauquet, C. M. & Bishop, D. H. L. (2000). Virus Taxonomy: Classification and Nomenclature of Viruses: Seventh Report of the International Committee on Taxonomy of Viruses. (October 2000), Academic Press, San Diego, USA.

Russel, W. B.; Saville, D. A. & Schowalter, W. R. (1989). *Colloidal Dispersions* (1st edition). Cambridge University Press, ISBN 9780521426008, New York, USA.

Saffari, H.; Malugin, A.; Ghandehari, H. & Pease III, L.F. (2012). Electrostatic Deposition of Nanoparticles into Live Cell Culture Using an Electrospray Differential Mobility Analyzer (ES-DMA). *J. Aerosol Sci.* (2012), in press.

Saucy, D. A.; Ude, S.; Lenggoro, I. W. & Fernandez de la Mora, J. (2004). Mass Analysis of Water-Soluble Polymers by Mobility Measurement of Charge-Reduced Ions Generated by Electrosprays. *Anal. Chem.* Vol. 76, No. 4, (January 2004), pp. 1045-1053.

Shoemaker, G. K.; Duijn, E. V.; Crawford, S. E.; Uetrecht, C.; Baclayon, M.; Roos, W. H.; Wuite, G. J. L.; Estes, M. K.; Prasad, B. V. & Heck, A. J. R. (2010). Norwalk Virus Assembly and Stability Monitored by Mass Spectrometry. *J. Mol. Cell Proteomics.* Vol. 9, No. 8, (April 2010), pp. 1742–51.

Siuzdak, G.; Bothner, B.; Yeager, M.; Brugidou, C.; Fauquet, C. M.; Hoey, K. & Change, C.-M. (1996). Mass Spectrometry and Viral Analysis. *Chem. Biol.* Vol. 3, No. 1, (January 1996), pp. 45–48.

Song, D. K.; Lenggoro, I. W.; Hayashi, Y.; Okuyama, K. & Kim, S. S. (2005). Changes in the Shape and Mobility of Colloidal Gold Nanorods with Electrospray and Differential Mobility Analyzer Methods. *Langmuir.* Vol. 21, No. 23, (November 2005), pp. 10375-10382.

Swann, M. J.; Peel, L. L.; Carrington, S. & Freeman, N. (2004). Dual-Polarization Interferometry: An Analytical Technique to Measure Changes in Protein Structure in Real Time, to Determine the Stoichiometry of Binding Events, and to Differentiate between Specific and Nonspecific Interactions. *J. Anal. Biochem.* Vol. 329, No. 2, (June 2004), pp. 190-198.

Thomas, J. J.; Bothner, B.; Traina, J.; Benner, W. H. & Siuzdak, G. (2004). Electrospray Ion Mobility Spectrometry of Intact Viruses. *Spectroscopy*. Vol. 18, No. 1, (January 2004), pp. 31–36.

Tsai, D. H.; Kim, S. H.; Corrigan, T. D.; Phaneuf, R. J. & Zachariah, M. R. (2005). Electrostatic-Directed Deposition of Nanoparticles on a Field Generating Substrate. *Nanotechnology.* Vol. 16, No. 9, (July 2005), pp. 1856-1862.

Tsai, D. H.; Zangmeister, R. A.; Pease III, L. F.; Zachariah, M. R. & Tarlov, M. J. (2008). Gas-phase Ion-mobility Characterization of SAM functionalized Au Nanoparticles. *Langmuir.* Vol. 24, No. 16, (July 2008), pp. 8483-8490.

Tsai, D. H.; Pease III, L. F.; Zachariah, M. R. & Tarlov, M. J. Aggregation Kinetics of Colloidal Particles Measured by Gas-phase Differential Mobility Analysis. *Langmuir.* Vol. 25, No. 1, (December 2008), pp. 140-146.

Tsai, D.H.; Lipin, D. I.; Guha, S.; Feldblyum, J. I.; Cole, K. D.; Brorson, K. A.; Zachariah, M. R.; Tarlov, M. J.; Middelberg, A. P. J. & Pease III, L. F. (2011). Process Analytical Technology for Recombinant Pandemic Flu Vaccines: Viral Ultrastructure, Aggregation, and Binding. *AIChE Annual Meeting.* CD-ROM. (2011), New York.

Umbach, P.; Georgalis, Y. & Saenger, W. (1998). Time-Resolved Small-Angle Static Light Scattering on Lysozyme During Nucleation and Growth. *J. Am. Chem. Soc.* Vol. 120, No. 10, (March 1998), pp. 2382-2390.

Wang, W. (2005). Protein Aggregation and its Inhibition in Biopharmaceutics. *Int. J. Pharm.* Vol. 289, No. 1–2, (January 2005), pp. 1–30.

Weisbecker, C. S.; Merritt, M. V. & Whitesides, G. M. (1996). Molecular Self-Assembly of Aliphatic Thiols on Gold Colloids. *Langmuir.* Vol. 12, No. 16, (August 1996), pp. 3763–3772.

Wick, C. H.; McCubbin, P. E. & Birenzvige, A. (2006). Detection and Identification of Viruses using the Integrated Virus Detection System (IVDS); ECBC Technical Report: 2006, ECBC-TR-463.

Wiedensohler, A. (1988). An Approximation of the Bipolar Charge-Distribution for Particles in the Sub-Micron Size Range. *J. Aerosol Sci*. Vol. 19, No. 3, (1988), pp. 387–389.

Yim, P. B.; Clarke, M. L.; McKinstry, M.; De Paoli Lacerda, S. H.; Pease III, L. F.; Dobrovolskaia, M. A.; Kang, H. G.; Read, T. D.; Sozhamannan, S. & Hwang, J. (2009). Quantitative Characterization of Quantum Dot-Labeled Lambda Phage for

Escherichia Coli Detection. *Biotechnol. Bioeng.* Vol. 104, No. 6, (December 2009), pp. 1059-1067.

Zhu, Z.; Anacker, J. L.; Ji, S.; Hoye, T. R.; Macosko, C. W. & Prud'homme, R. K. (2007). Formation of Block Copolymer-Protected Nanoparticles via Reactive Impingement Mixing. *Langmuir.* Vol. 23, No. 21, (September 2007), pp. 10499-10504.

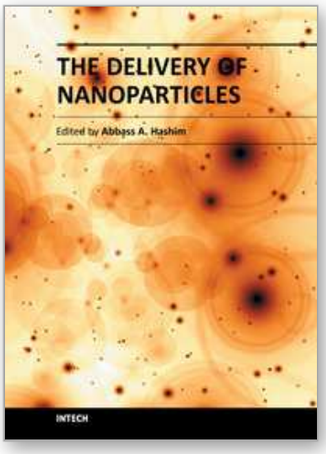

The Delivery of Nanoparticles

Edited by Dr. Abbass A. Hashim

ISBN 978-953-51-0615-9
Hard cover, 540 pages
Publisher InTech
Published online 16, May, 2012
Published in print edition May, 2012

Nanoparticle is a general challenge for today's technology and the near future observations of science. Nanoparticles cover mostly all types of sciences and manufacturing technologies. The properties of this particle are flying over today scientific barriers and have passed the limitations of conventional sciences. This is the reason why nanoparticles have been evaluated for the use in many fields. InTech publisher and the contributing authors of this book in nanoparticles are all overconfident to invite all scientists to read this new book. The book's potential was held until it was approached by the art of exploring the most advanced research in the field of nano-scale particles, preparation techniques and the way of reaching their destination. 25 reputable chapters were framed in this book and there were alienated into four altered sections; Toxic Nanoparticles, Drug Nanoparticles, Biological Activities and Nano-Technology.

How to reference

In order to correctly reference this scholarly work, feel free to copy and paste the following:

Rajasekhar Anumolu and Leonard F. Pease III (2012). Rapid Nanoparticle Characterization, The Delivery of Nanoparticles, Dr. Abbass A. Hashim (Ed.), ISBN: 978-953-51-0615-9, InTech, Available from: http://www.intechopen.com/books/the-delivery-of-nanoparticles/rapid-nanoparticle-characterization

INTECH
open science | open minds

InTech Europe
University Campus STeP Ri
Slavka Krautzeka 83/A
51000 Rijeka, Croatia
Phone: +385 (51) 770 447
Fax: +385 (51) 686 166
www.intechopen.com

InTech China
Unit 405, Office Block, Hotel Equatorial Shanghai
No.65, Yan An Road (West), Shanghai, 200040, China
中国上海市延安西路65号上海国际贵都大饭店办公楼405单元
Phone: +86-21-62489820
Fax: +86-21-62489821